Wake Blockage Corrections and Ground Effect Testing in Closed Wind Tunnels

J. E. Hackett* and R. A. Boles†
Lockheed-Georgia Company, Marietta, Ga.

A new method for estimating blockage corrections is described which relates wall static pressure measurements at the test section entry and exit directly to the interference velocities experienced at the model. Model, rig, and power effects are included. Using this method, tests on a 20 in. jet flap model in a 42 in. wide tunnel correlated well with "free air" results in a large tunnel. The highest test lift coefficient was 15 and a moving ground was used. Theoretical and experimental studies are described concerning the use of a tangentially blown wind tunnel floor to replace a moving ground. Tests on the above model, at one chord altitude, confirm the feasibility of this approach. Applications of the new procedures are described and discussed.

Nomenclature

$\mathcal{R}$ = aspect ratio
A_T = cross-sectional area of test section
C = wing chord
C_D = drag coefficient
C_L = lift coefficient
$C_{L_{hb}}$ = lift coefficient based on area between wing and ground
C_P = pressure coefficient
C_{REF} = reference chord
C_μ = momentum coefficient
C_l = section lift coefficient based on wing chord
C_{l_h} = section lift coefficient based on height above ground
D = drag
d = jet diameter
H = height of jet above ground
h = height of wing quarter chord above ground
KBF = knee-blown flap
L = jet half-width
N = wall jet blowing constant
n = blockage correction factor
P = pressure
Q = source
q = dynamic pressure
Re = Reynolds number
S = wing area
t = ground blowing slot height
U = velocity or induced velocity (horizontal)
V_j = jet velocity
V_{SLOT} = ground blowing slot velocity
V = velocity or induced velocity (vertical)
V_B = blocked velocity
V_{CAL} = calibrated velocity
V_M = velocity at the model
X = distance from jet virtual origin
α = angle of attack
δ = conventional boundary correction factor
η = spanwise station
ρ = air density

Subscripts

1 = conditions at pressure orifice at upstream end of contraction
2 = conditions at pressure orifice at downstream end of contraction
M = conditions at model location
NOM = nominal
TE = trailing edge
∞ = freestream

Presented as Paper 74-641 at the AIAA 8th Aerodynamic Testing Conference at Bethesda, Md., July 8-10, 1974; submitted February 3, 1975; revision received October 20, 1975.

Index categories: Aircraft Aerodynamics (including Component Aerodynamics); Airfract Performance; VTOL Testing.

*Scientist. Member AIAA.

†Aerodynamics Engineer, Senior.

I. Introduction

LARGE scale wind tunnel tests on powered STOL models can experience at least two major difficulties in establishing confidence in the results. The first concerns the application of wind tunnel blockage corrections ("we never use them for powered models"). The second problem arises during ground effects testing over a nonmoving tunnel floor or ground board which frequently is the only option at large scale. Here, ground (or tunnel floor) separation can invalidate the results of high lift tests.

The first half of this paper describes work directed at the tunnel blockage for centrally mounted powered models. Though considerable effort has been expended during the past decade on wall interference corrections for powered models, very much less can be found in the literature concerning their blockage effects, which are at least as important. Accordingly, an opportunity was taken to make measurements in a large (23¼ × 16¼ ft) and in a small (42 × 30 in.) wind tunnel using a 20 in. span model designed for very high lift. The results are described in Secs. II and III, together with a new wake blockage correction method which relates interference at the model directly to static pressures measured at orifices mounted in the tunnel walls, roof, and floor.

The second half of the paper concerns ground effects testing, which is also described in Ref. 1-3. The problem is addressed of simulating a moving ground without actually having one. This is most desirable because of the logistic and operational problems associated with the belt type of moving ground at large scale. Theoretical and experimental studies are described in Sec. IV concerning ground effect and its simulation using a moving ground and via a newly developed boundary-layer control scheme.

II. Tunnel Blockage Estimation for Powered and Unpowered Models

A. Conventional Blockage Corrections

The presence of a viscous wake with a positive displacement thickness reduces the effective tunnel cross-sectional area downstream of a wind tunnel model. This increases the mean velocity in the downstream part of the test section and a portion of this increase is felt at the model. The purpose of blockage corrections is to remove this effect. A second, essentially inviscid class of wake blockage effects concerns solid

blockage and somewhat analogous flow around closed separation bubbles. Model volume and base pressures are used for estimating these effects. References 4-7 describe the conventional techniques in general use.

For unpowered models, viscous wake blockage corrections should be based on skin friction contributions including the model and its supports and (strictly) should include the effects of any changes in tunnel wall skin friction caused by model-induced pressures. In practice, rig drags are usually estimated and model skin friction is obtained by subtracting lift-dependent drag from total drag. Induced drag at zero lift (caused by wing twist, for example) and due to lateral forces thus sometimes incorrectly become included during blockage estimation. Changes in tunnel wall friction are never included.

For blockage correction purposes, the body is replaced by a source of strength Q ft^3/sec (see Fig. 1), at the model location, together with appropriate sets of images in the same cross-sectional plane. The images have no direct effect at the model. To satisfy continuity, a sheet of sinks is introduced at infinity downstream which induces a super-velocity aft of the model equal to Q divided by tunnel area. At the model, half this value is taken in classical correction theory.

For powered models, it is usually assumed that a jet acts like a "negative wake" and the same procedure is used. However, though a jet does indeed introduce blockage, there exist both geometric and fluid-mechanical differences between jet and wake flows which make the conventional negative wake approach inappropriate.

B. Power Effects

In order to typify the general characteristics of powered models, let us first consider the simplified case of a jet exhausting horizontally. It is well known that the far field outside of a circular jet exhausting into quiescent free air may be represented by a line sink extending from the orifice to downstream infinity. In the confines of a wind tunnel and at low forward speed this representation remains valid for a short distance downstream, after which spreading is accelerated via the influence of image sinks (ejector effect). However, the replacement of the point sink of conventional theory by a line sink increases the (negative) blockage effect because of a direct contribution from the image sinks. The one-half factor clearly is no longer appropriate. The factor will also change depending upon whether the jet geometry is axisymmetric or two-dimensional, for example. In the limit, with entrainment effects concentrated predominantly far aft of the model, the conventionally calculated blockage correction could be doubled by this effect.

Another aspect of the same problem concerns the mixing properties of jets and wakes, which determine their effective sink strengths. Figure 2, which is adapted from Ref. 9, shows the variation of jet half-width with excess velocity ratio. The half-width has been normalized on x, the distance from the jet virtual origin. Points on this plot may be regarded either as describing the same jet at successive streamwise distances or as initial conditions for differing jets. A jet in a slow stream ("A" in the figure) spreads almost in proportion to x (i.e., L/x is nearly constant). As the excess velocity diminishes (approaching "B"), spreading becomes less rapid and the effective sink strength is reduced. If, alternatively, "A" and "B" are regarded as separate jets which have differing exit velocities at the model, we see that the average spreading rate for "B" is the smaller. We also note that, at a particular absolute value of the velocity ratio, the spreading rate of a wake‡ (e.g., at C) is greater than that for a jet. The fact that Fig. 2 is not symmetric about the origin thus demonstrates that a jet cannot be regarded simply as a negative wake, even in free, incompressible flow.

The discussion so far has centered mainly upon simple, axisymmetric jets and wakes; even for these, it has become

‡Note that, in order to show continuity of the curve through the origin, L/x has been assigned negative values for wakes.

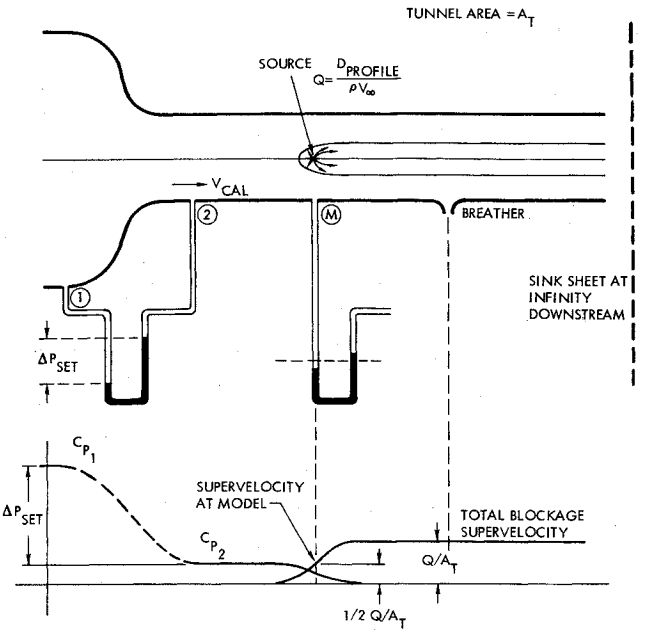

Fig. 1 Conventional blockage assumptions.

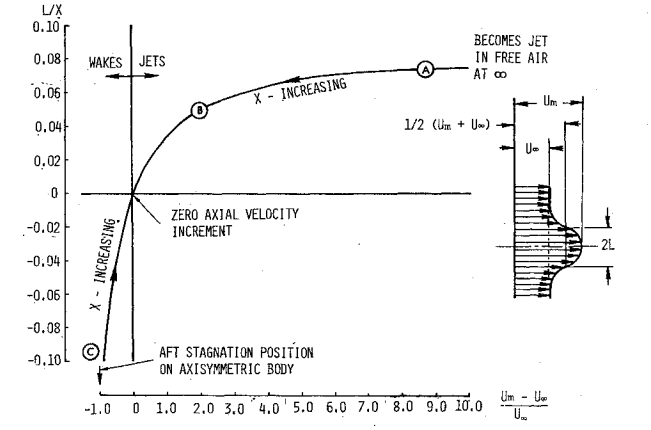

Fig. 2 Growth characteristics of axisymmetric jets and wakes.

clear that the application of blockage corrections to powered models is no longer straightforward. In high lift testing, further complications are added, such as unconventional nozzles, including jet flaps; jets inclined at large angles to the flow; thick, viscous wakes in proximity to jets; etc. Tunnel floor skin friction, compared with the situation during calibration, is also highly modified when a moving ground is needed during ground effects testing. The chances appear slim for extending conventional blockage corrections successfully under conditions such as these.

C. Direct Method for Blockage Estimation

It is evident that a blockage correction method is needed which is direct in the sense that all of the complications above can be accommodated without specific attention to detail. The possibility of determining blockage experimentally is therefore considered.

If it were practical, a velocity and total pressure survey could be made in the entire working section, and a detailed, equivalent theoretical blockage body could be constructed, centered about the various wake and jet centerlines emanating from the model and with the equivalent jet cross sections being of negative area. A detailed image system would then provide not only the mean blockage effect, but also its distribution across and along the working section. Such a system is, of course, neither practical nor necessary. First, a mean effect is generally sufficient, and, second, com-

prehensive pressure measurements are not required because wall static pressures reflect equivalent information, provided they can be measured and properly interpreted.

Perhaps the most obvious place for wall static pressure measurements is in the same cross-sectional plane as the model (see "M" in Fig. 1). These are probably necessary to estimate solid or bubble blockage effects, but are not required for the viscous-wake-related blockage effects which will be treated in the present paper.

At some distance downstream from the model, the only significant model-induced flow effects (other than blockage) at the tunnel walls are due to the trailing vortex system. This induces components normal to the mainstream direction which affect wall static pressures very little. In many tunnels the breather slot is situated at an appropriate station and, in fact, defines this mean static pressure. Positive blockage is then felt as an above atmospheric absolute pressure at working section entry (2 in Fig. 1). This is readily measureable on most tunnel systems using the working section entry piezometering.

The correction to dynamic pressure is then obtained as follows: mainstream volume flow at "2" (Fig. 1) = $V_{CAL}A_T$ and mainstream area opposite to breathers = $A_T - (Q/V_{CAL})$, where Q is the total source strength between "2" and the breather. Hence, opposite to the breather

$$V_B = \frac{V_{CAL}A_T}{A_T - (Q/V_{CAL})} \simeq V_{CAL}\left(1 + \frac{Q}{V_{CAL}A_T}\right) \tag{1}$$

giving $\Delta C_{P_2} = 2Q/A_T V_{CAL}$ to first order, where ΔC_{P_2} is measured, blockage-induced change in static pressure coefficient at "2" (Fig. 1), above the tunnel-empty (calibration) condition. Using

$$V_M = V_{CAL} + n\frac{Q}{A_T} \tag{2}$$

we obtain

$$\frac{V_M}{V_{CAL}} = 1 + \tfrac{1}{2}n\Delta C_{P_2} \tag{3}$$

or

$$\frac{\Delta q}{q} = n\Delta C_{P_2} \text{ to first order} \tag{4}$$

For wake contributions, experience has shown point sinks to be successful, using $n = \frac{1}{2}$. For jets, we saw in the previous section that larger values are implied by line-sink entrainment effects. However, this effect is attenuated when the breather or equivalent downstream measurement station is situated not far aft of the model. Pending experimental evidence to the contrary, $n = \frac{1}{2}$ will be taken, giving the blockage correction:

$$\frac{\Delta q}{q} = \tfrac{1}{2}\Delta C_{P_2} \tag{5}$$

Since the above method relies upon measurements of far upstream and far downstream conditions, the corrections obtained apply only to streamlined flow wake blockage. Solid body blockage and that due to bubble-type separations, not detected by the present method, may be obtained conventionally. Work is currently in progress to determine these, too, via analogous measurements of wall static pressures.

III. Tunnel Blockage Experiments

A. Wind Tunnel Model and Equipment

Figure 3 shows a 20 in. span, knee-blown jet flap wing model tested at the Lockheed-Georgia Company. The model

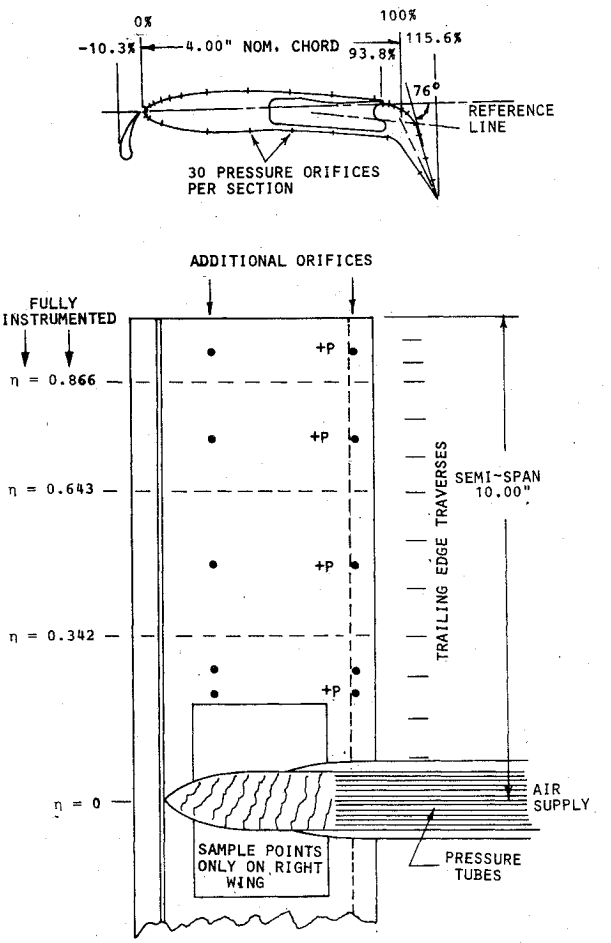

Fig. 3 The knee-blown flap (KBF) model.

was designed for basic studies at very high lift and is described in detail in Ref. 10. Testing was carried out in the Research Low Speed Wind Tunnel (see Fig. 4) and in the 23¼ × 16¼ ft wind tunnel. The latter "free air" results and test/analysis procedures are reported in Ref. 10. All of the data in this section are derived from wing surface pressure measurements and include estimated slat loads.

In the smaller tunnel, a moving ground was run at mainstream speed to prevent floor separation at the higher lift ranges. The model was centrally mounted. The tunnel was run at a contraction pressure drop corresponding to 5 psf dynamic pressure with working section empty. Only the side pressure orifices were used at the working section entry and their reading was recorded independently of the upstream value.

B. Test Results

Figure 5 shows a comparison between lift performance of the *KBF* model in the small and large ("free air") wind tunnels. The excellent high lift capability of the model is also evident. The fact that flow remained fully attached along the entire $C_\mu = 5.8$ curve testifies to the effectiveness of the slat. Of the maximum "free air" lift coefficient of about 14, about 8.5 can be attributed to circulation lift. Under this condition, the front stagnation point had moved back below the flap knee.

In the smaller tunnel, the high lift results are marked by a sudden rise in lift, starting at between 12 and 16 degrees of incidence. It is in this range that the upper surface of the flap swings through the vertical position, and it appears that the jet flips forward, just above the moving ground, as illustrated in Fig. 6. Forward moving jet fluid eventually escapes sideways, around the edges of the floor pressure footprint, creating considerable viscous losses and blockage. The $C_{\mu_{NOM}} = 6.0$ curve in the lower part of Fig. 7, which shows a

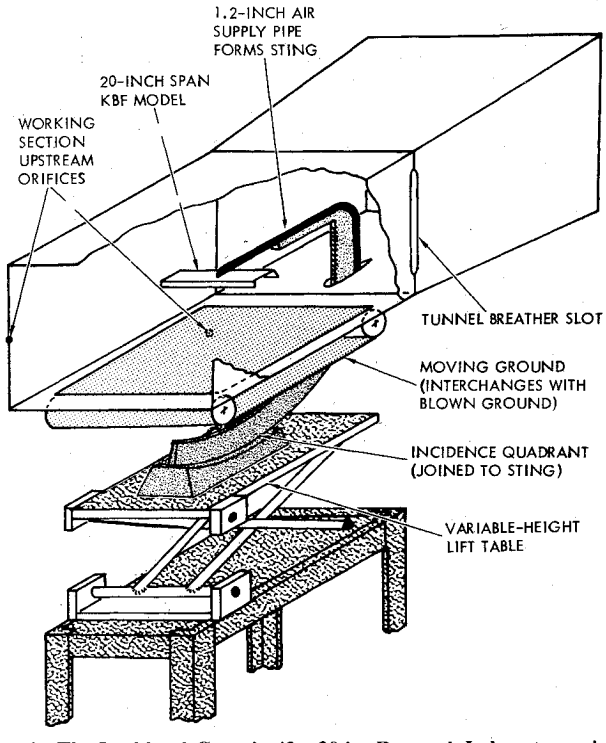

Fig. 4 The Lockheed-Georgia 42×30 in. Research Laboratory wind tunnel (conceptual sketch).

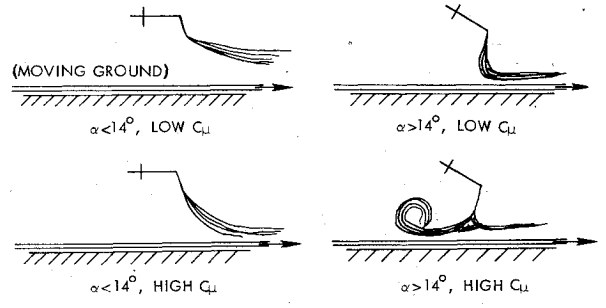

Fig. 5 Lift performance of the KBF model.

corresponding static pressure rise at working section entry, confirms this explanation.

At lower incidences, it was evident that the jet sheet exerted a strong pumping action on the working section flow. It was necessary to reduce tunnel fan rpm quite appreciably in order to hold speed under these conditions.

C. Application of Wind Tunnel Constraint Corrections

A significant difficulty in assessing the success of wind tunnel corrections concerns the separation of lateral (lifting) constraint effects from longitudinal (blockage) ones. Fortunately, the upstream pressure measurements just described demonstrate an obvious and easily recognizable example of wind tunnel blockage. Nevertheless, to check the success of the method, a suitable set of incidence corrections also must be made.

Since the model is reasonably small (47.5% of tunnel width) and employs uniform, full-span blowing, a conventional, powered model incidence correction may be used. Thus

$$\Delta\alpha = \frac{\delta}{1+(2C_\mu/\pi AR)}\frac{S}{C}C_L \tag{6}$$

$$\Delta C_L = -C_L \cdot \tfrac{1}{2}\Delta C_{P_2} - C_D\Delta\alpha \tag{7}$$

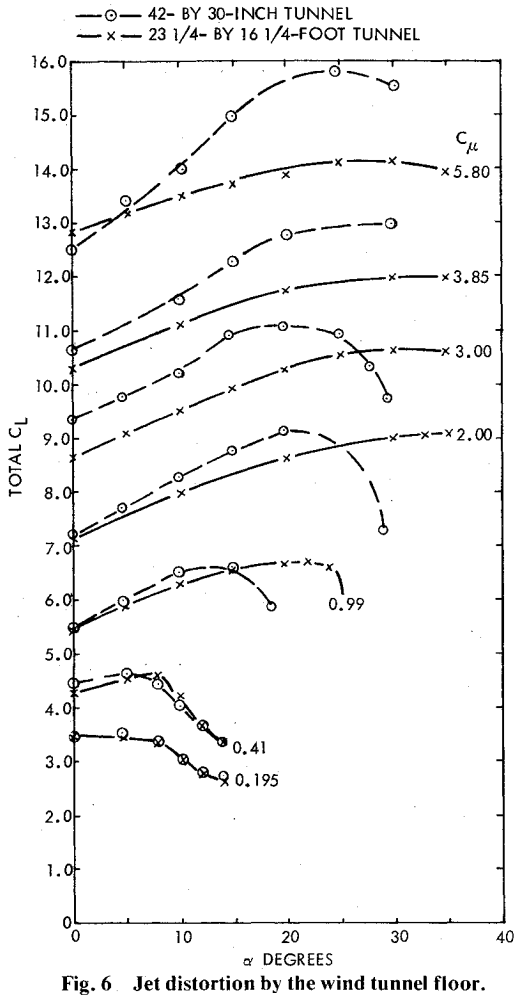

Fig. 6 Jet distortion by the wind tunnel floor.

$$\Delta C_D = -C_D \cdot \tfrac{1}{2}\Delta C_{P_2} + C_L\Delta\alpha \tag{8}$$

$$\Delta C_\mu = -C_\mu \cdot \tfrac{1}{2}\Delta C_{P_2} \tag{9}$$

Figure 8 shows the results of this procedure, applied to the basic data of Fig. 5. The method is evidently quite successful. The only significant exception occurs at $C_\mu = 3$. Here, closer studies showed that the small tunnel results are inconsistently high and are probably in error. It should be remarked that the jet becomes sonic at the slot exit somewhere near $C_\mu = 3$.

The success of the present wake blockage corrections (Fig. 8) is attributable to lack of significant bubble-type separations under high lift conditions. Had these been present, the differences between tunnels would have been even larger and the above correction method would have removed only the blockage effect associated with wake total pressure losses.

IV. Moving Ground Simulation

A. Basic Flows

In two-dimensional potential flow a wing experiences increasing ground-image-induced, counter-to-mainstream flow as the ground is approached or as circulation is increased. This reduces the available lift below the free air value and eventually a limiting value is reached (see Fig. 9 and Ref. 1). Approaching the ground still closer, or by some means increasing wing circulation, then yields decreasing lift until counterflow nullifies the mainstream velocity and zero lift results.

In three dimensions, the above effects are halved at the tip and there follows a tendency for the span load shape to flatten. The action of the trailing vortex system tends to oppose this trend.

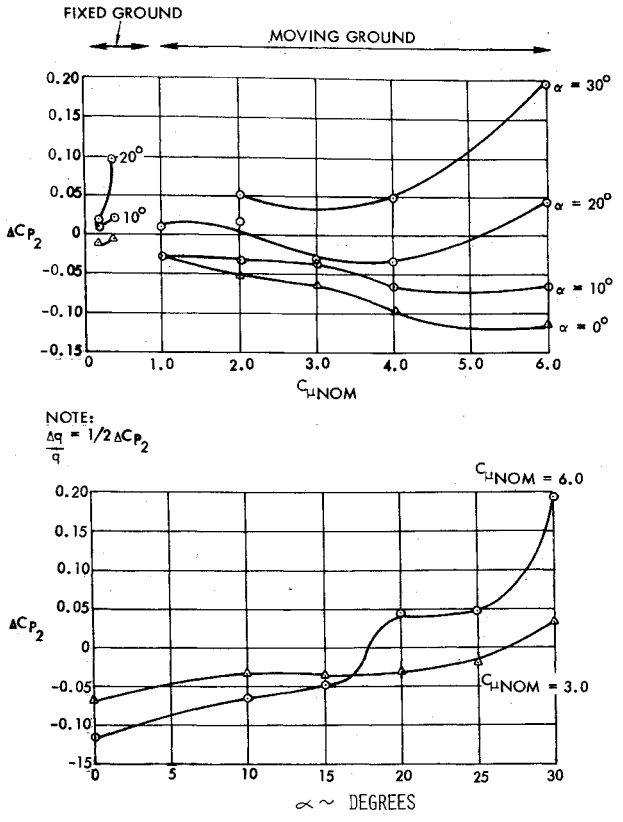

Fig. 7 Measured static pressures at working section entry (small tunnel): side wall orifices only.

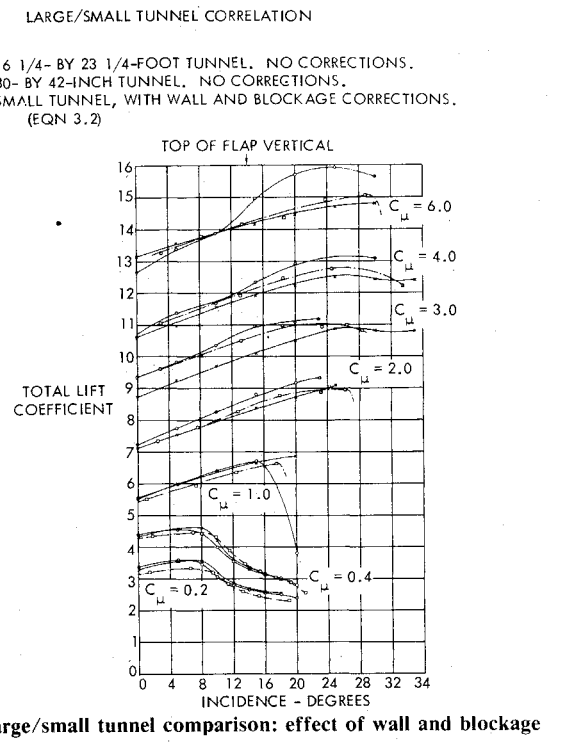

Fig. 8 Large/small tunnel comparison: effect of wall and blockage corrections.

It is obvious, and well known, that a wind tunnel fixed ground experiences separation long before the above tendencies can be measured; this has brought the moving ground into use. Even with a moving ground, however, "separation" can and should occur at sufficiently high lift (see Fig. 9, lower part).

Figure 10(a) shows an experimentally observed flow, using the model described in Sec. III situated above a moving ground. The figure combines the results of surface pressure measurements and flow visualization of several kinds. It is evident that, even with a moving ground, a trapped vortex occurs. Figure 10(b) shows that the mechanism of ground-induced lift loss is via undersurface suctions induced by this vortex. With a fixed ground (0% belt speed), the loss is greatly magnified by premature separation. In this high lift regime a moving ground is evidently necessary in order to position the ground stagnation points correctly so that proper undersurface interference occurs. Any device designed to replace a moving ground must also have this property.

Though it is not currently possible to theoretically investigate viscous flows with a trapped vortex, a quite extensive investigation was made into prestagnation boundary-layer flows[1] so as to provide a better understanding of the problem. Figure 11a shows calculated displacement thickness beneath an idealized horseshoe vortex situated above a fixed ground. Lift is almost sufficient to precipitate separation. The strong fore-aft symmetry of the displacement surface is quite remarkable and is caused by a corresponding fore-aft symmetry in the ground pressure distribution (which is typical), coupled with an almost elastic response of the boundary layer (at least at this low Reynolds number). Because of the fore-aft symmetry of the boundary layer displacement surface, the wing experiences increased local velocity and positive flow cambering. However, it experiences very little incidence change. This is perhaps contrary to expectation. At higher Reynolds numbers, the aft thinning of the boundary layer is more marked and some induced incidence effects should be expected. Figure 11b shows the results of a similar computation for a moving ground boundary layer. Though the physical thickness is, of course, positive, the displacement thickness is now negative. This is because the belt moves faster than the flow immediately above it (which is retarded by the action of the bound vortex) and consequently entrains air via viscous action. The effect is automatically greatest where the static pressure maximized and can be thought of as self-optimizing boundary-layer control. Once again, fore-aft symmetry occurs in the displacement surface and there is little incidence change induced at the model. For the moving ground, however, the effective velocity at the model is reduced (slightly) and negative flow cambering occurs. For both the fixed and moving ground boundary layers, Fig. 11 shows that displacement thickness represents only a small portion of model height, even at low Reynolds number.

B. Tangential Blowing as a Replacement for Moving Ground

In principle, a constant peak velocity, equal to mainstream speed, could be maintained by using a series of slots blowing tangentially along the wind tunnel floor. However, the use of

Table 1 Boundary-layer-induced velocities at model

	C_{l_h}	Fixed Ground		Moving Ground		Blown Ground	
		Low Re*	High Re+	Low Re	High Re	Low Re	High Re
v/U_∞ (Vertical)	1.0	+.0014	+.0010	-	-	-	-
	2.0	(S)	-.0010	-.0001	+.0024	+.0003	-.0002
	3.0	(S)	(S)	-.0001	+.0038	-.0004	-.0009
	4.0	(S)	(S)	+.0001	+.0047	-.0011	-.0017
u/U_∞ (Horizontal)	1.0	+.0123	+.0065	-	-	-	-
	2.0	(S)	+.0200	-.0017	-.0026	-.0012	-.0014
	3.0	(S)	(S)	-.0005	-.0005	-.0065	-.0065
	4.0	(S)	(S)	-.0125	-.0098	-.0180	-.0183

*Re = 0.35 X 10^6 +Re = 9.86 X 10^6 (S): Separated

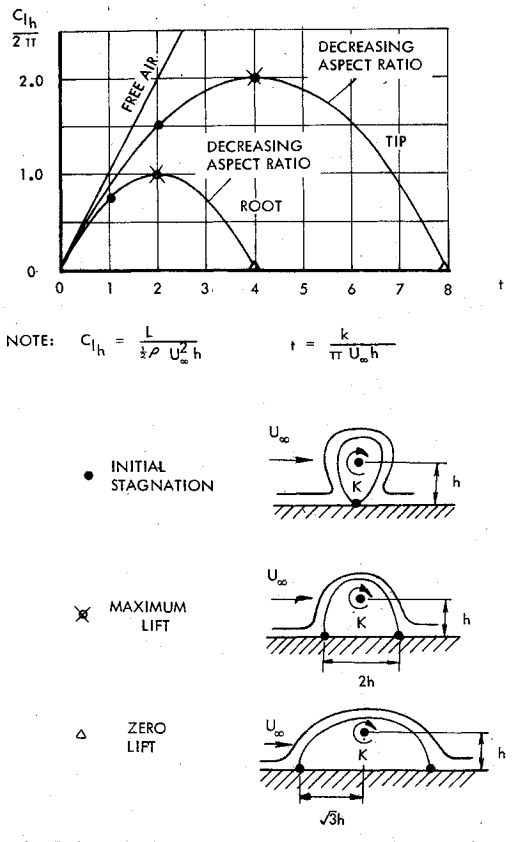

Fig. 9 Lift reduction by the ground image of a bound vortex.

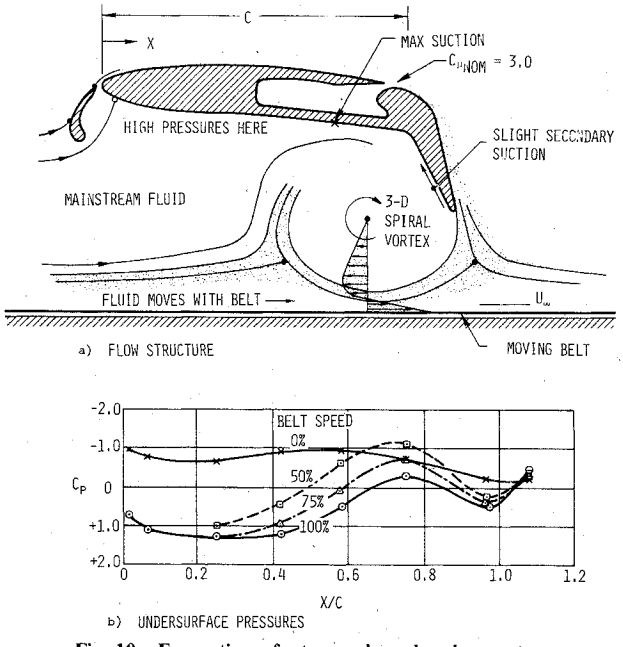

Fig. 10 Formation of a trapped, underwing vortex.

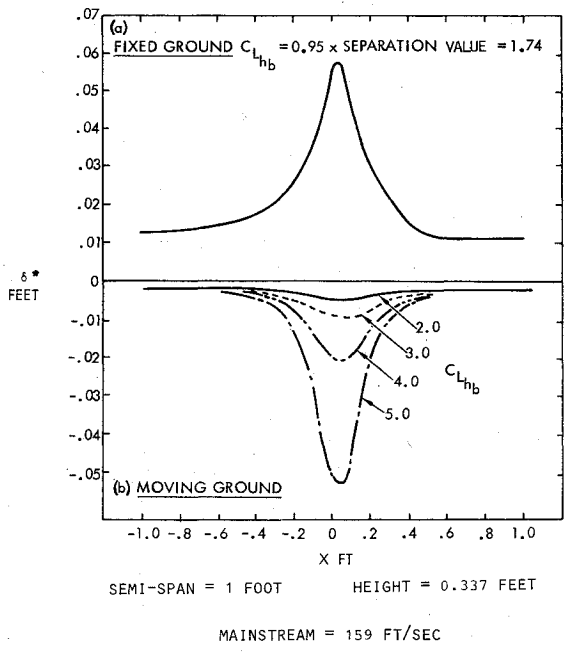

Fig. 11 Calculated boundary-layer displacement thickness on fixed and moving grounds.

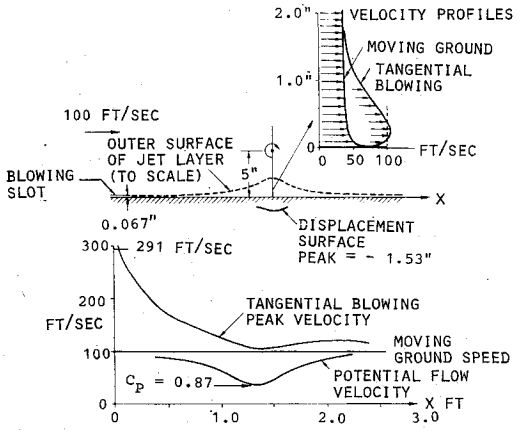

Fig. 12 Application of ground tangential blowing at $C_{L_h} = 4.0$.

a single properly sized and positioned slot is more desirable. A series of theoretical calculations was therefore made[1] to provide a baseline for experimental studies.

Figure 12 includes the geometry of a possible ground tangential blowing scheme designed for use with the KBF model. It will be noted that the peak velocity remains fairly constant for some distance fore and aft of the model position. However, the velocity profile differs markedly from that for a moving ground and, in fact, has about sixteen times the (negative) displacement thickness of the corresponding moving ground boundary layer. Whether this matters can be determined by calculating displacement effects but ultimately must be decided by experiment. Table 1 summarizes calculated values of boundary-layer displacement-surface-induced velocities, at the model, for three varieties of simulated ground. The large disparity in displacement thickness is not reflected in the displacement-surface-induced velocities because the model-induced changes in displacement thickness are similar for moving ground and tangentially blown boundary layers. The latter have a large, constant component of displacement thickness. The results shown in Table 1 were sufficiently encouraging for confirmatory experiments, extending into the post-separation C_L range, to be undertaken.

C. Tangentially Blown Ground Experiments

Individually controlled tangential blowing slots were constructed in the floor of the 30×42 in. wind tunnel. Suitable static and skin-friction instrumentation permitted checks to be made against theoretical predictions. Slot blowing velocities were calculated using the equation:

$$U_{SLOT} = U_\infty \left(1 + \frac{N}{2\pi} C_l \frac{h}{C}\right) \tag{10}$$

where N is a constant determined from wall jet calculations to lie in the range $2 < N < 3$.

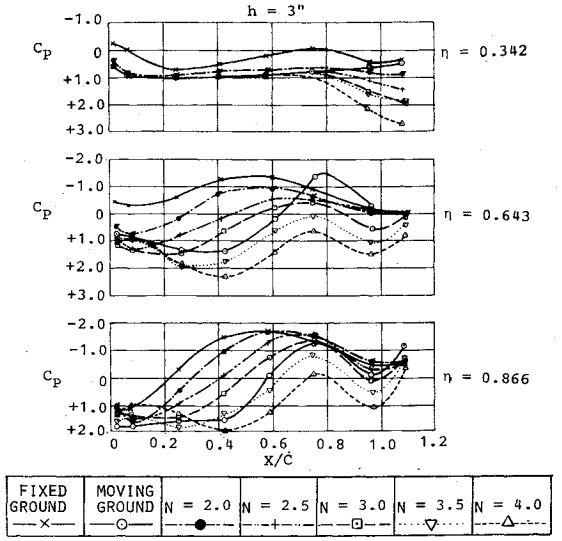

Fig. 13 Effect of ground tangential blowing on wing lower surface pressures. $C_{\mu_{Nom}} = 3.0$, $\alpha = 0°$.

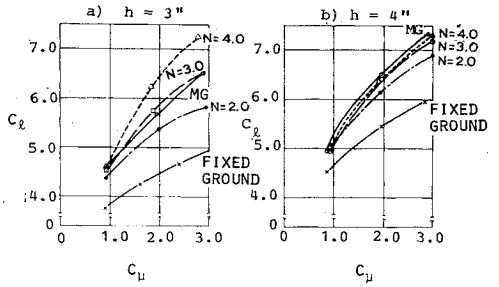

Fig. 14 Local lift coefficients for various ground simulation techniques, $\eta = 0.643$.

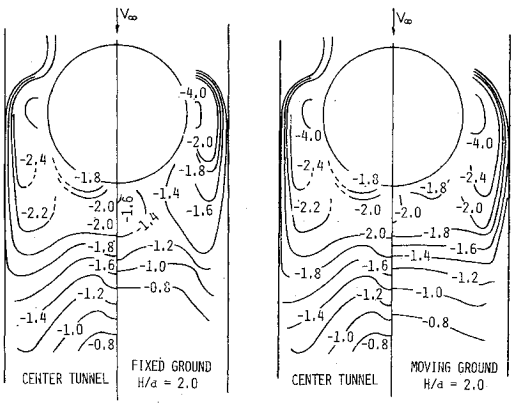

Fig. 15 Distortion of jet exit plane pressure distributions in ground effect, $V_j/V_\infty = 5.0$.

Experiment showed that, for most conditions of interest, a slot two chords ahead of the quarter-chord line was optimum. Figure 13 shows typical underwing pressure distributions for various N values and for fixed and moving ground conditions. It is clear that proper flow conditions are achieved with the ground tangentially blown, even with a trapped vortex present. Extensive additional tests confirmed these results over ranges of model height, blowing level, and slot gap and position.[2] Figure 14 shows local lift coefficients corresponding to the $\eta = 0.643$ curves of Fig. 13. These values exclude slat loads, which were shown to be small for the present, zero-incidence tests. The corresponding free-air total lift coefficient (see Fig. 8) is approximately 5.5 at unit C_μ, rising to 8.6 at $C_\mu = 3$. A detailed study over this range[2] for $h = 3$ in. shows that fixed ground lift errors may be reduced from as much as -1.5, in C_L, to ± 0.2 by the use of floor blowing

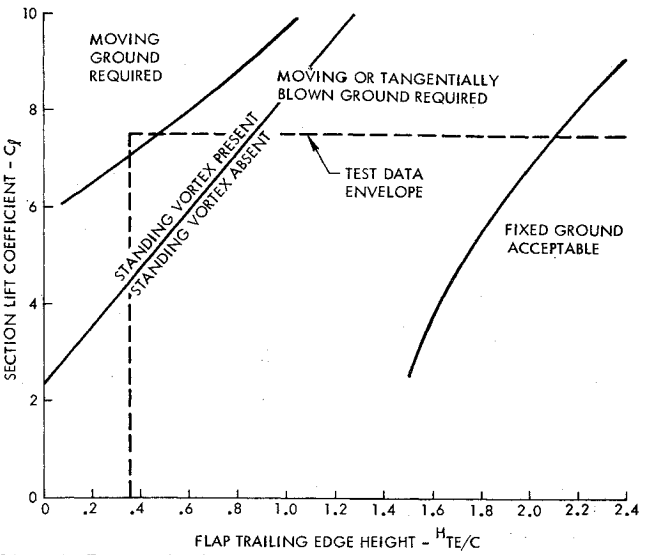

Fig. 16 Boundaries for the use of a tangentially blown floor: wing lift critical.

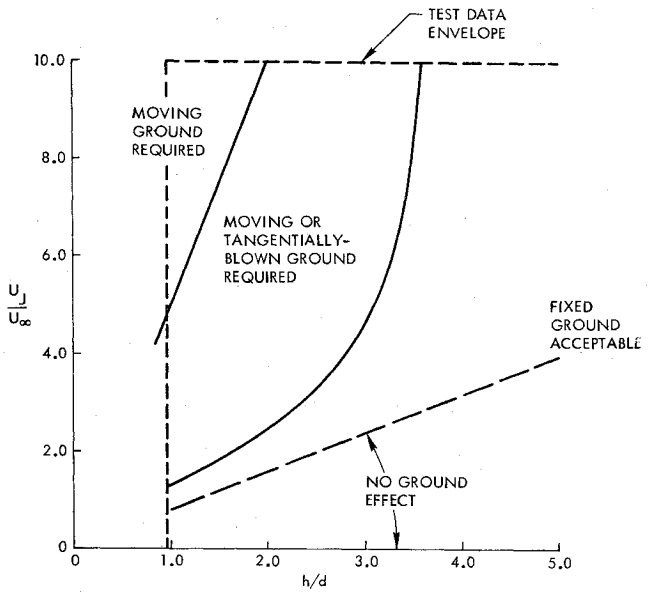

Fig. 17 Boundaries for the use of a tangentially blown floor: jet lift critical.

with $N = 3$. At 4 in. altitude (one nominal chord) a similar effect is observed with $N = 2$, 3, or 4.

As a point check on the wider applicability of the floor tangential blowing scheme, limited tests were carried out on a model with a 1.75 in. diam. round jet exhausting vertically from the bottom of a 2.75 in. wide fuselage.[2] Figure 15 shows that, even under quite extreme conditions, the errors due to ground separation are likely to be much less than previously. In fact, there was no measurable ground effect when $U_j d/U_\infty H$ was less than 1.25. Between 2.5 and 5 tangential blowing was decreasingly successful, and beyond this it appears that a moving ground should be used. However, this extreme condition would occur very rarely during routine testing.

The following equations summarize floor tangential blowing requirements found during experiments described previously. The quoted C_μ values are defined two-dimensionally. Experiments with reduced-width moving belts show that slot widths need not exceed model span.

$$C_{\mu_{slot}} = \frac{\frac{1}{2}\rho_{slot} U_{slot}^2}{\frac{1}{2}\rho_\infty U_\infty^2} \cdot \frac{t}{C_{REF}} \left\{ 1 + N \frac{C_{\nu_h}^{\ 2}}{2\pi} \right\} \qquad (11)$$

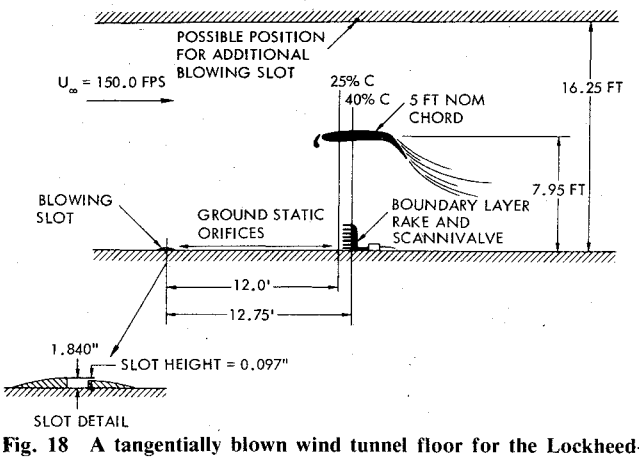

Fig. 18 A tangentially blown wind tunnel floor for the Lockheed-Georgia 23¼ × 16¼ ft wind tunnel.

With ground separation present

$$C_{\mu_{slot}} = 0.088 \frac{c}{h} (C_{\ell_h} - 3.5) \tag{12}$$

For a round jet

$$C_{\mu_{slot}} = 0.027 C_{\ell_h} \tag{13}$$

where $C_{\ell_h} = C_\ell c/h$ and t is slot height

Where $N=2$, Eqs. (11) and (12) indicate very similar slot blowing requirements. As both are supported by experimental results, this gives confidence in the soundness of the underlying theory for predominantly attached ground flow.

D. Operating Boundaries for Ground Effects Testing

Though many V/STOL configurations have generally similar ground flow patterns at high lift, the range of configuration variables is too large for more than a general indication of operating boundaries to be given. On the basis of tests described previously wing-dominant and jet-dominant cases may be identified, however. Figures 16 and 17 show the respective boundaries deduced from test observations.

V. Application

A. Wind Tunnel Blockage Constraint Measurements

These measurements are basically straightforward, following the lines set out previously. In cases where tunnel breathers are not situated at the downstream end of the working section, it is suggested that pressures should be measured at an equivalent cross section. These should be on the vertical walls only, with possibly three orifices per wall. A more comprehensive set of orifices is currently being mounted in the Lockheed-Georgia Research Laboratory wind tunnel. Some of these are distributed along the working section length and will be used in connection with car testing.

In the Research Laboratory wind tunnel, "corrected q" running capability is now provided without resort to a digital computer. Since the corrections of Eqs. (4) and (5) are simple functions of measured pressures, it is relatively straightforward to set up an analog circuit to provide a "corrected q" reading at the tunnel console.

Although a relatively simple form of lateral constraint correction was used previously, larger or more complicated models generally will not permit this. In such cases, care may be needed to avoid overlap between calculated and measured constraint corrections.

B. Moving Ground Simulation

Though the present results permit estimation of ground-blowing C_μ's over a fairly wide range of conditions, it is not very desirable, from an operational standpoint, to attempt pre- or real-time calculations of slot blowing pressure. Figure 18 shows a more practical scheme, in which floor boundary layer rake measurements are employed to set a blowing pressure which gives the correct velocity maximum (i.e., equal to mainstream). This particular arrangement was designed for center-tunnel testing in the Lockheed-Georgia Research Low Speed Wind Tunnel and has been employed there in two-dimensional tests. The blowing position above the model is aimed at avoiding roof separation where the static pressure recovers to the freestream value. Since the pressure gradients concerned are likely to be very similar to those on the floor ahead of the model, it appears reasonable to use an identical slot and tee into a common supply.

The requirement for most center-tunnel testing is to prevent tunnel floor separation, rather than size a trapped vortex properly (see Fig. 10 and Section IV). In such cases, the instrumentation could probably be reduced safely to Preston (skin-friction measuring) tubes or even wool tufts.

VI. Conclusions

1) Wind tunnel blockage corrections for streamline flow may be estimated via wall static pressure measurements at working section entry and exit using simple relationships [see Eqs. (4-9)]. The method does not allow for solid or bubble-type wake blockage effects.

2) The method has been applied successfully in jet-flapped model tests up to a lift coefficient of fifteen and a blowing momentum coefficient of six, with attached flow.

3) Pitching moment corrections may reflect blockage gradient; this topic requires further work.

4) Under most circumstances ground effects testing may be successfully accomplished using tangential blowing at the floor to replace a moving ground. The method has been applied successfully in jet flapped model tests, at an altitude of ¾ chord, well into the flow regmine in which a trapped underwing vortex is present with a moving ground. Success was also achieved with a round lifting jet model.

5) Both methods are simple to apply and each complements the other. It is conjectured that, once deeper insight is gained into bubble-separation blockage and into pitching moment aspects, they will permit larger models to be used in existing hard-walled wind tunnels than previously could be tested with confidence.

References

[1]Hackett, J.E. and Praytor, E.B., "Ground Effect for V/STOL Aircraft Configurations and Its Simulation in the Wind Tunnel. Part I—Introduction and Theoretical Studies," NASA CR 114, 495, Nov. 1972.

[2]Hackett, J. E., Boles, R. A., and Praytor, E. B., "Ground Effect for V/STOL Aircraft Configurations and Its Simulation in the Wind Tunnel. Part II – Experimental Studies," NASA CR 114, 496, Nov. 1972.

[3]Hackett, J. E., Praytor, E. B., and Caldwell, E. O., "Ground Effect for V/STOL Aircraft Configurations and Its Simulation in the Wind Tunnel. Part III – Application to the NASA-Ames 40- by 80-foot Wind Tunnel," NASA CR 114, 497, Nov. 1972.

[4]Herriot, J. G., "Blockage Corrections for Three Dimensional-Flow Closed-Throat Wind Tunnels With Consideration of the Effect of Compressibility," NACA TR 995, 1950.

[5]Thom, A., "Blockage Corrections in a High Speed Wind Tunnel," Aeronautical Research Council, R&M 2033, 1943.

[6]Pope, A., *Basic Wing and Airfoil Theory*, McGraw-Hill, New York, 1951.

[7]Glauert, H., "Wind Tunnel Interference on Wings, Bodies, and Airscrews," Aeronautical Research Council, R&M 2566, 1933.

[8]Hackett, J. E. and Boles, R. A., "Wind Tunnel Techniques and Operational Boundaries for STOL Testing," Lockheed-Georgia Company, Marietta, Ga., Engineering Report LG73ER0004, Jan. 1972.

[9]Vogel, W. M., "Exact Solution of Growth Parameters for Two-Dimensional and Axisymmetric, Self-Preserving Turbulent Jets and Wakes," Report 68-5, McGill University, Montreal, Canada, Aug. 1968.

[10]Hackett, J. E. and Lyman, V., "The Jet Flap in Three Dimensions: Theory and Experiment." AIAA Paper 73-653, Palm Springs, Calif., 1973.

[11]Hackett, J. E. and Evans, M. R., "Vortex Wakes Behind High Lift Wings," *Journal of Aircraft*, Vol. 8, May 1971, pp. 334-340.